PLANETARY SCIENCE

Persistence of intense, climate-driven runoff late in Mars history

Edwin S. Kite[1]*, David P. Mayer[1†], Sharon A. Wilson[2], Joel M. Davis[3], Antoine S. Lucas[4], Gaia Stucky de Quay[1,5‡]

Mars is dry today, but numerous precipitation-fed paleo-rivers are found across the planet's surface. These rivers' existence is a challenge to models of planetary climate evolution. We report results indicating that, for a given catchment area, rivers on Mars were wider than rivers on Earth today. We use the scale (width and wavelength) of Mars paleo-rivers as a proxy for past runoff production. Using multiple methods, we infer that intense runoff production of >(3–20) kg/m^2 per day persisted until <3 billion years (Ga) ago and probably <1 Ga ago, and was globally distributed. Therefore, the intense runoff production inferred from the results of the Mars Science Laboratory rover was not a short-lived or local anomaly. Rather, precipitation-fed runoff production was globally distributed, was intense, and persisted intermittently over >1 Ga. Our improved history of Mars' river runoff places new constraints on the unknown mechanism that caused wet climates on Mars.

INTRODUCTION

Emerging theories for planetary climate evolution (*1*) can be tested using the geologic record of Mars' prolonged wet-to-dry climate transition. This transition has been argued to result from atmospheric loss processes that would have been most intense <0.5 billion years (Ga) after Mars formed [e.g., (*2*)] and to have been aided by the shutdown of Mars' geodynamo. However, >1 Ga after Mars formed and ≳1 Ga after Mars' geodynamo failed, the planet was still intermittently scoured by precipitation-fed water runoff (*3*, *4*). These late-stage (mainly ~3.6 to 2 Ga) rivers and lakes, whose deposits have been explored in situ at one site by the Mars Science Laboratory rover (*5*), required more water than could have been produced by the direct effect of asteroid impacts (*6*). To the contrary, these rivers and lakes record a late-stage river-forming climate (or climates), which is a challenge for models. The late-stage climate (or climates) allowed up to 1 km of fluvial incision [averaged over the scale of O(10^2) km^2 of alluvial fan source catchments; (*7*, *8*)] but was more arid and/or had shorter wet periods than the earlier river-forming climate that cut the regionally integrated valley networks (*9*). Moreover, late-stage deep fluvial erosion involved shorter rivers that were more spatially concentrated than were the earlier planet-spanning regionally integrated valley networks (*10*, *11*). Given these data, and the great difficulty of accounting for intense climate-driven runoff late in Mars history when the atmosphere is thought to have been thin, it is reasonable to expect that the late-stage climate had less intense runoff production (kilograms of discharge per square meter of catchment area per day; also written as millimeters per hour) or only yielded intense runoff in a few places. Such a record of waning peak runoff would be fully consistent with the mineralogical record (*12*) and with the expectation from models that Mars' surface energy balance increasingly inhibits runoff as the atmosphere is lost (*13*).

This hypothesis of waning peak runoff can be tested by combining measurements of paleochannel size [a proxy for discharge Q (*14*)] and measurements of channel catchment area, A. Then, $Q/A = R$, where R is the runoff production. The higher the value of R, the more stringent is the constraint on surface energy balance and thus on climate models. Given the importance of R as a constraint on climate models, it is perhaps surprising that so few measurements relevant to Mars' runoff production have been made [e.g., (*15*); see the Supplementary Materials]. Even fewer data exist for the late-stage rivers. This is, in part, because reliable picking of channel widths and slopes requires high-resolution stereo digital terrain models (DTMs): Only a few suitable Mars DTMs are publicly available. Moreover, many >3 Ga old paleochannels on Mars have been eroded to the point where present-day width provides little constraint on the width of the original channel: In some cases, even the original channel slope and catchment area cannot be measured from orbit. Last, discharge estimates based on channel dimensions show order-of-magnitude scatter [e.g., (*14*)]. Together, these issues weaken the usefulness of any single-channel measurement and define the challenge for a global survey.

MATERIALS AND METHODS

We carried out a globally-distributed survey for well-preserved late-stage paleochannels with catchments of known area, aided by a global database of Mars alluvial fans and deltas (*16*) and including many previously reported sites. In addition to image data, our survey (see the Supplementary Materials) made use of 39 High Resolution Imaging Science Experiment (HiRISE) DTMs and numerous Context Camera (CTX) DTMs, with 30 newly constructed HiRISE DTMs used for this project (table S1) (*17*). Measurements were carried out on orthoimages with a typical resolution of 0.5 m per pixel, and typical channel widths in our database are 50 to 100 m; therefore, features are well resolved (>100 pixels per width) (figs. S1 and S2). Although many channels are too eroded for reliable measurements, hundreds of channels and channel deposits are well preserved in map view. Good preservation is enabled by Mars' slow dry-era wind erosion and tectonic quiescence. For many Mars' river deposits, slow erosion of floodplain deposits leaves channels and lateral accretion

[1]University of Chicago, Chicago, IL, USA. [2]Center for Earth and Planetary Studies, Smithsonian Institution, Washington, DC, USA. [3]Natural History Museum, London, UK. [4]Institut de Physique du Globe de Paris, Centre National de la Recherche Scientifique, Paris, France. [5]Imperial College London, London, UK.
*Corresponding author. Email: kite@uchicago.edu
†Present address: United States Geologic Survey, Astrogeology Science Center, Flagstaff, AZ, USA.
‡Present address: Department of Geological Sciences, University of Texas at Austin, Austin, TX, USA.

deposits preserved in inverted relief (*18*, *19*). In many cases, Mars' inverted channels are better preserved in map view (both in scale and in sedimentary detail) than for any location on Earth (fig. S1). River channel–fill deposit width records past bankfull width [e.g., (*20*)]. Mars images show single-thread sinuous channels, and evidence for braided rivers has not been reported from Mars orbiter data. This is unexpected because the steep slopes of Mars rivers and the (presumed) absence of plant roots on Mars would both lead us to expect braided rivers, which are ubiquitous for Earth's Precambrian (*21*). To prevent the single-thread channels from widening to form braided rivers, a bank-strengthening agent (e.g., clay) was required (*22*). To focus on channels whose dimensions are a proxy for past climate, we excluded channels likely formed by release of subsurface water, channels formed by single floods, and almost all channels downstream of lake-overflow breaches. The database is biased toward late-stage deposits (Late Hesperian and earliest Amazonian, 3.4 to 2 Ga; see the Supplementary Materials for chronology discussion). This is mainly because only well-preserved channels are included, and preservation quality decreases with increasing age. We found well-preserved late-stage paleochannels that are globally distributed, spanning elevations of +2 to −5 km and latitudes of 41°S to 52°N (Fig. 1). Regions poleward of 60° in both the northern and southern hemispheres were excluded from the analysis because they have been resurfaced by glacial and periglacial processes. Because most slopes are <2° (fig. S3), the ~3.6 to 2 Ga water-carved paleochannels are easily distinguished from steep , <10-million-year-old (Ma) gullies, which terminate on >10° slopes, are usually smaller in scale, and which may result from dry processes (*23*). On the basis of geologic context and examination of high-resolution images, 87% of channels in our database modify sedimentary deposits, and the remaining 13% rework ancient crustal materials of unknown origin (table S2).

We reduced the data using a procedure modified after (*24*) (see the Supplementary Materials for details). Sinuous channel centerlines were traced in triplicate. Where multiple segments with well-preserved widths existed for the same channel, the corresponding results were averaged. The yield is a set of channel widths (n = 205) and sinuous channel wavelengths (n = 104) for Mars paleochannels draining 154 catchments of known area.

RESULTS

Rivers on Mars were wider than rivers on modern Earth

Paleochannel widths for Mars (Fig. 2) plot at or above the upper limit of the envelope of the largest available database of bankfull widths and catchment areas for Earth's rivers [the U.S. compilation of (*25*)]. This Earth database spans a wide range of climate zones and tectonic environments. In the 10^2 to 10^3 km^2 catchment area range for which we have the most data, the Mars paleochannels are >2× wider than are the Earth channels. The existence of inverted channels provides an internal cross-check on these measurements (fig. S2). Because dry-era erosion narrows the flat-topped ridges that preserve inverted channels but widens negative relief channels, the true paleochannel widths are probably more than the widths of the inverted channels but less than the widths of the negative relief channels

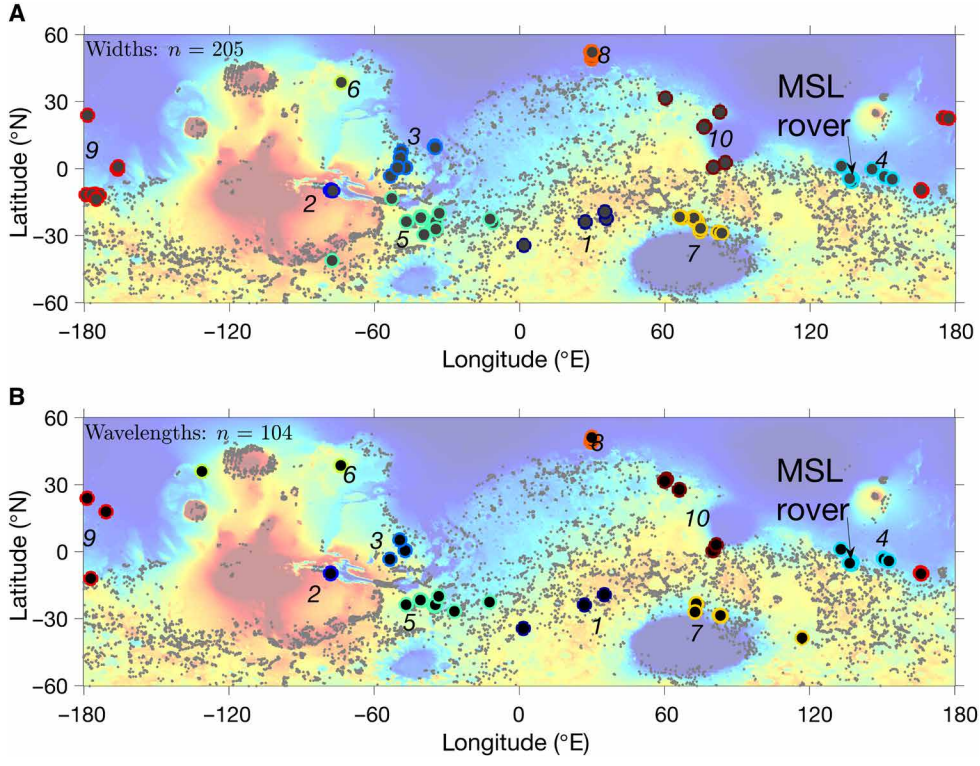

Fig. 1. Global distribution of data. Most of our data are for post–3.4 Ga rivers. Width (**A**) and wavelength (**B**) measurements. Some measurements are too close-spaced to be distinguished at this scale. We use *k*-means clustering of spatial locations of the data (see the Supplementary Materials) to identify 10 distinct groups, labeled 1 through 10. Each group is represented by circles of varying colors. Location of the Mars Science Laboratory (MSL) rover shown for reference. For comparison, the gray dots show the location of (mostly pre–3.4 Ga) valleys mapped by (*11*). The background is Mars Orbiter Laser Altimeter topography, clipped at elevations of −6 km (blue) and 8 km (red).

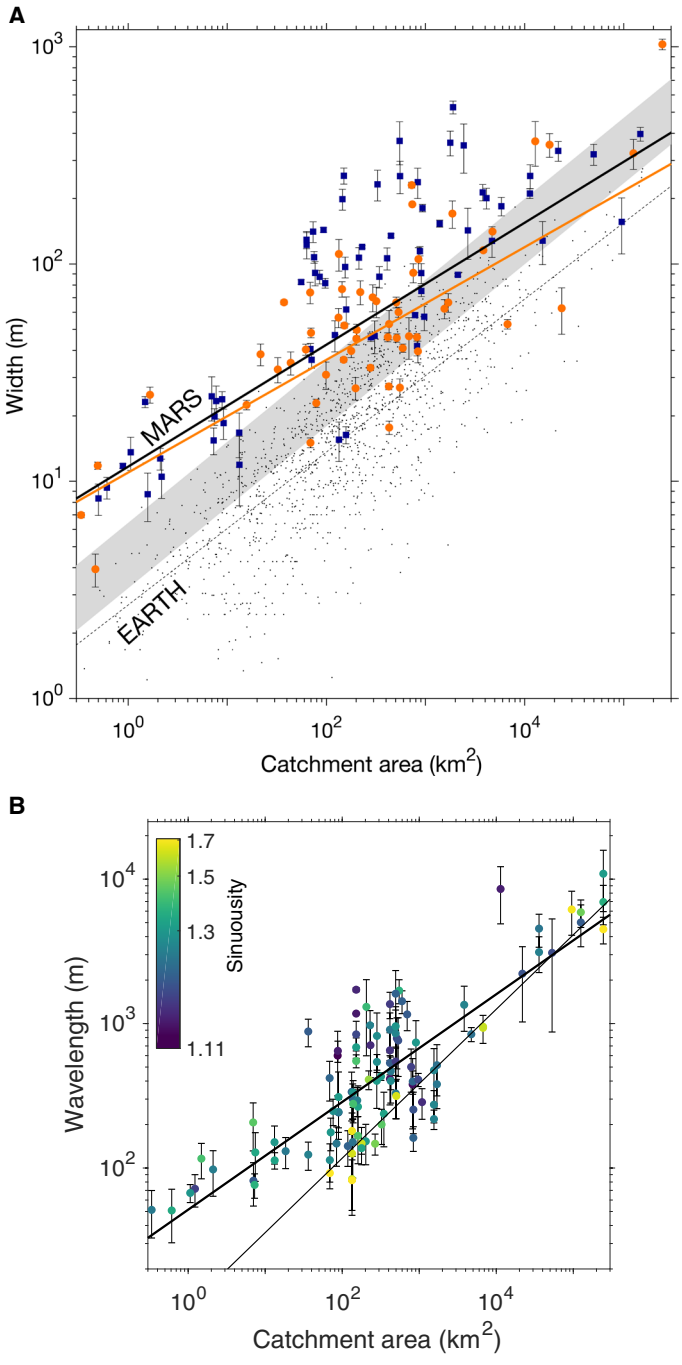

Fig. 2. Mars paleo-river dimensions. (**A**) River width comparison for ancient Mars versus modern Earth. Mars data are shown using colored symbols (blue squares, negative relief channels; orange circles, inverted relief channels). The thick black line is the best fit to all Mars data, and the thick orange line is the best fit to Mars inverted relief channel widths. Only the widest channel for each catchment area is shown. The gray-shaded region corresponds to the channel widths expected based on the best-fit to meander wavelengths 0.0625 × to 0.125 × wavelength (*19*). Earth data (*25*) are shown as black dots, and the best fit to Earth data are shown by the thin dashed line. (**B**) Mars sinuous channel wavelengths. Color of dots corresponds to sinuosity. The thick black line shows the fit to all data. The thin black line shows the fit to the most sinuous channels (sinuosity >1.5).

(consistent with data; Fig. 2). The inverted relief channels preserve more diagnostic texture than the negative relief channels, which helps to confidently measure channel width. A second independent cross-check on the measurements comes from meander wavelengths. Mean meander wavelength is proportional to channel width on Earth, which can be understood in terms of growth of river bars to form bends (*26*). Meander wavelength cannot be greatly altered by erosion. The width trend predicted by the trend of meander wavelengths (gray shaded band in Fig. 2A; see also Fig. 2B) is close to the measured widths of the inverted relief channels, as expected. After fitting for catchment area, the remaining scatter does not exceed the natural variability observed on Earth (black dots in Fig. 2A). The observation that Mars paleochannels are wider than Earth rivers cannot be altered by considering all of the rivers in a catchment; nor by excluding alluvial fan data from the fit; nor by considering only the very best preserved rivers (fig. S4); and nor by excluding any one geographic region from the fit. Because our DTMs and anaglyphs have vertical precision of ~1 m or even better, we were able to avoid measuring strath terraces and multistory channel sandbodies, but we cannot rule out the possibility that some of our inverted channel widths correspond to channel amalgamations (not paleochannels). Nevertheless, the insensitivity of the fit to the preservation quality "cut," and the agreement of the meander wavelengths with typical width/wavelength ratios on Earth, implies that such mismeasurements are not a severe problem. Most of the channels in our database are not steep enough to be debris-flow chutes (fig. S3). Karst-like widening of paleochannels cannot explain large meander wavelengths nor wide inverted channels. Inverted relief channels, for a given catchment area, are about twice as wide as Earth rivers. Therefore, we conclude that, for a given catchment area, rivers on Mars were wider than rivers on Earth.

Evidence for intense, globally-distributed climate-driven runoff persisting late in the great drying of Mars

River deposit width and river deposit wavelength can both be used to estimate river discharge Q (*14*, *27*, *28*). Because sediment transport increases nonlinearly with increasing discharge, river channels are shaped by flood runoff, not by the annual mean runoff production. Typically, river channel–forming discharges are similar to or greater than the median year's annual maximum in river discharge. For estimating past river discharge on Mars, two methods have been used. One discharge estimation method uses empirical correlations between channel dimensions and discharge, usually with a correction for Mars' gravity (*14*, *15*, *18*, *19*). This predictor has a per-channel SE of a factor of $^5/_3$ in discharge when tested using the Earth data of (*25*). The second method sets river depth slightly above that needed for gravity-dependent basal shear stress (τ) to mobilize river-bed material ($\tau \approx \tau_{cr}$) (*29*, *30*). This second method requires slope information and an (assumed) grain size. The first method may be a better estimate because it reproduces observed width-to-depth ratios for terrestrial rivers (*31*, *32*) and "because the [Mars] deposits could record transport conditions well above threshold," among other reasons (*14*). Published work on Earth's permafrost-river hydraulic geometry does not support a large permafrost correction for width (fig. S8) (*33*). We emphasize the biggest-in-catchment widths because our alluvial fan rivers may subdivide downstream of the fan apex.

The resulting discharges are shown in Fig. 3 (see the Supplementary Materials for details of method). For the second method, we use

slope information from our DTMs (table S1), and our starting point is to assume bedload transport of gravel (*5*), with a log-uniform prior on typical grain diameter D_{50} between 0.01 and 0.5 m. This is conservative because assuming suspension transport of sand would predict higher discharges. River-transported boulders with a size of >0.75 m would be resolved by full-resolution HiRISE images but are only rarely seen on Mars. We also show discharge estimates for the range of grain diameter inferred by (*34*) for an exceptionally well-preserved late-stage fluvial deposit.

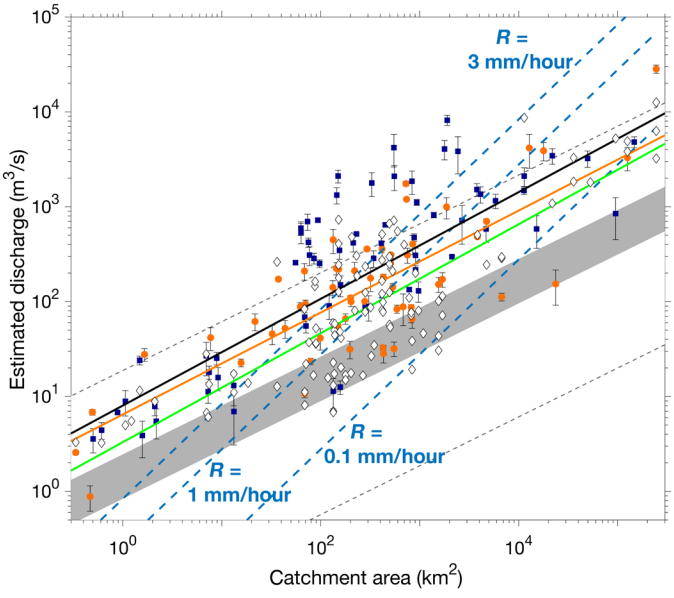

Fig. 3. Paleodischarge estimates. Filled symbols are width-based discharge estimates using an empirical scaling. Blue squares, negative relief channels; orange circles, inverted relief channels. Open diamonds are meander-wavelength based discharge estimates, using an empirical scaling (error bars not shown). The blue dashed lines show runoff production, *R*. The black line shows the fit to the width data, the orange line shows the fit to the inverted relief channels only, and the green line shows the fit to the sinuous-channel wavelength data. The gray band shows the fit to the data re-estimated using a scaling that is strongly dependent on grain size for $D_{50} \approx 0.0625$ to 0.125 m (*34*). The gray dashed lines show fits to the width data for the extremes of the range of D_{50} considered, $D_{50} = 0.01$ to 0.5 m. All wavelengths are shown, but only the largest widths in each catchment are shown. The bootstrap errors on the fits are small and are not shown.

Next, we divide the discharge by catchment area to get runoff production, *R*. The data show a reduction in catchment-averaged runoff production with increasing catchment area (Fig. 3). This is the expected result of unsteady or patchy runoff production and is also observed on Earth (fig. S5). The catchment-averaged runoff production estimates are high (Fig. 4). These values are conservative in terms of local maximum runoff production and melt/rain rates because infiltration, evaporation/refreezing, and unsteady runoff production are all likely and all tend to reduce the contribution of rainwater and meltwater to river discharge. High *R* is consistent with past rainfall on Mars (*35*) because snowmelt runoff production is restricted by an energetic upper limit that does not apply to rainfall. Rainfall is the return to the ground of water from the atmosphere, water that was gathered by the atmosphere over large scales of space and time. By contrast, snowmelt production is local and limited by the local surface energy balance. The evidence for rainfall is not decisive however. For example, if grain size on Mars was at the low end of our D_{50} range, then modest river depths could transport sediment, so discharge could be small for a given river width. [Fine grain size is likely to be the explanation for the exceptionally high runoff production inferred for $A < 3$ km^2. Catchments with $A < 3$ km^2 in our database are all located in the Southwest Melas canyon interior, region 2 in Fig. 1, whose geologic history suggests that rivers reworked fine-grained airfall deposits (*36*)]. Moreover, the preferred orientation of alluvial fan alcoves (*16*) suggests a runoff production mechanism that responds to insolation, such as seasonal melting (*37*).

Therefore, we express the implications of our runoff production constraint for climate evolution models (Fig. 4; our plot aggregates all runoff production estimates from our database) in terms of surface energy balance for snow/ice at the melting point. For snow/ice melt production, if ΔE is the additional energy (in watts per square meter) needed for runoff production, then $\Delta E \geq \rho RL$ (where $\rho = 1000$ kg/m^3 is the water density and $L = 334$ kJ/kg is the latent heat of melting). This ΔE requirement should also be satisfied by a climate

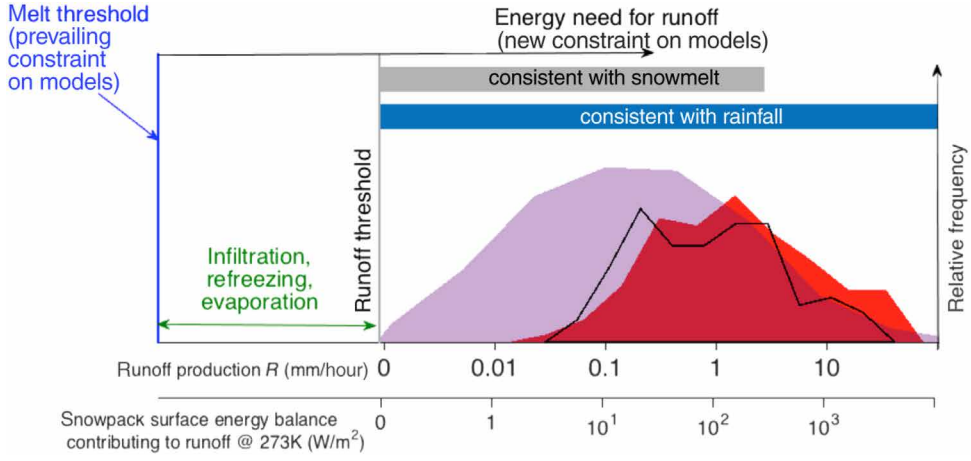

Fig. 4. Improved Mars paleoclimate model constraints via paleodischarge estimates from global database of paleo-rivers and river deposits. Results for all data are shown (not just the largest in each catchment). Additional energy generates runoff. Purple shading: width-based estimates, threshold channel method ($\tau = \tau_{cr}$); red shading: width-based estimates (empirical scaling); black line: meander-based estimates (empirical scaling). Because of geologic noise [e.g., (*14*)], the central estimate from the histograms (not the extremum) should be taken as the constraint for climate models.

that allowed rain because rainfall on Mars requires high annual mean temperatures (*38*). Thus, the observation of young rivers indicates that the energy balance has to permit snowmelt. The large size of the rivers that we have documented requires that models of late-stage climate not only warm snow temperature up to the melting point but also provide extra energy for melting, a further >(3–20) kg/m^2 per day (≡0.1 to 1 mm/hour), corresponding to 10 to 100 W/m^2 (Fig. 4). This ΔE must be added to the energetic cost of maintaining snow temperature at the melting point, which is $\sigma T_{melt}^4 > 300$ W/m^2, neglecting (likely large) heat losses to the atmosphere and the subsurface. The day-averaged absorbed solar energy at 20°S on 3 Ga Mars did not exceed 200 W/m^2, according to standard solar models. The large size of the rivers in our database, and the need to overcome snowpack "cold content" to allow infiltrating meltwater to produce runoff without refreezing (*39*), indicates that the runoff was not restricted to ephemeral noontime melting but was instead associated with day-averaged temperatures close to or above the freezing point, as on Earth. The need for a strong greenhouse effect is clear. However, this challenge is not met by most existing models of Mars' planetary climate evolution (see Discussion).

Geologic history of Mars' river runoff

Regional variations in channel width and wavelength can mostly be explained by regional variations in the catchment area (fig. S6). Unexpectedly, there is no evidence for a trend in peak runoff production with geologic age (Fig. 5A). Overall, runoff production in our mainly Late Hesperian and Amazonian dataset is comparable to the runoff production inferred previously for rivers that formed around the Noachian/Hesperian boundary (fig. S7) (*15*). Those Noachian/Hesperian boundary rivers were also precipitation fed (*40*). Moreover, the youngest region in our database (region 8, the <1 Ga rivers interior to Lyot) (*41*) plots above the trend line (Fig. 5A and fig. S6). We infer that climate-driven runoff that was both intense and globally distributed persisted late in the history of the drying out of Mars (Fig. 5). Late-stage runoff occurred over times spanning >(100–300) Ma (*8*), >2 Ga if Lyot is considered. The number, time separation, and

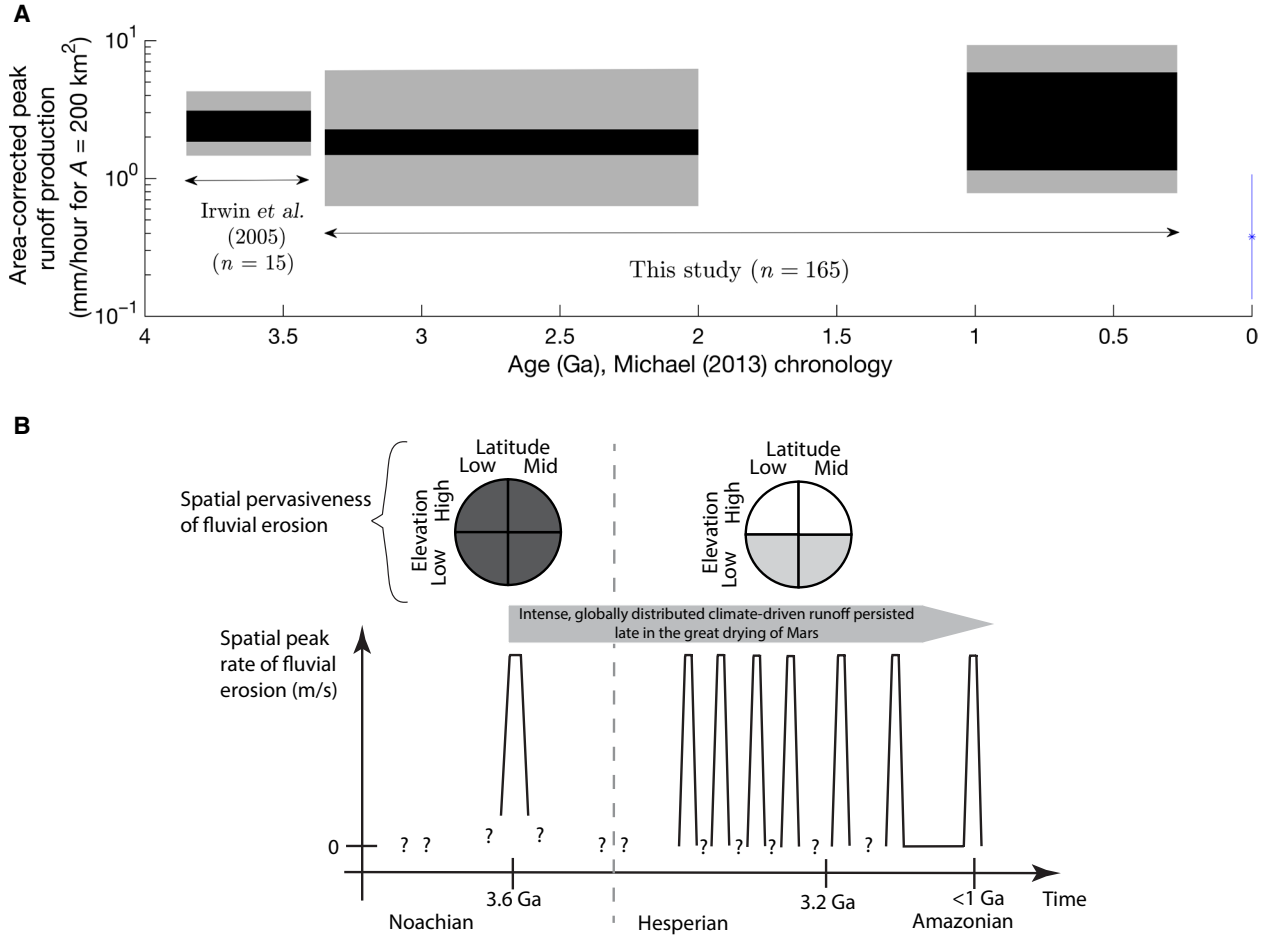

Fig. 5. A new geologic history of Mars' river runoff. (**A**) Our data are evidence that high rates of peak runoff production, and thus high peak rates of landscape erosion via fluvial sediment transport, were sustained after 3.4 Ga ago. The gray patches correspond to the catchment-to-catchment SD of the estimated runoff production, and the black bars correspond to the bootstrapped 2σ Poisson error for mean runoff production. The leftmost bar corresponds to results previously reported in (*15*). The central bar corresponds to our data for Late Hesperian/Early Amazonian terrains (with "highlands" measurements excluded; n = 149). The rightmost bar corresponds to our data for the (likely ice-rich) Middle Amazonian stippled mantling unit of Lyot crater (region 8 in Fig. 1; n = 16) (*41*). For our data, only the largest channels for each catchment are included. All data are corrected for the area dependence in runoff production seen in Fig. 3 (see fig. S7 for the uncorrected data). The offset between Earth's runoff production (blue symbol) and Mars' runoff production is sensitive to the assumed grain size (Figs. 3 and 4). (**B**) Summary of fluvial climates on Mars, informed by our results. Gray shading in upper quarter-circle plots corresponds to the spatial density of rivers (darker shading = higher spatial density).

cumulative duration of the Late Hesperian/Amazonian wet episodes remain poorly constrained (*8*). However, because of erosional exhumation by wind, our measurements sample many stratigraphic levels, and so intense runoff production must have occurred repeatedly through this interval (Fig. 5).

Relative to the Noachian/Hesperian boundary runoff, which was widely distributed in elevation (Fig. 1) (*11*), evidence for later-stage runoff is less spatially pervasive and is found preferentially at low elevations (Fig. 5). Although we did not find a correlation of R with elevation, >95% of the width data points fall below 0 km relative to the geoid (median, −1.5 km). Neither the Gale-Aeolis-Zephyria region targeted by Mars Science Laboratory nor the Isidis region (to be explored by the Mars 2020 rover component of the Mars Sample Return campaign) shows anomalously high runoff production relative to the planet-wide trend (fig. S6).

Given our result that younger rivers had as high runoff as earlier rivers, it is perhaps unexpected that earlier valleys include much more frequent lake overflows (*9*). This suggests that individual runoff-producing climates after 3.5 Ga either (i) lasted fewer years or (ii) had shorter melt seasons or fewer rainstorms, relative to the Noachian/Hesperian boundary river-forming climate. That would give correspondingly more time for water loss to evaporation and thus lower the chances of lake overspill. The first hypothesis predicts that only small (and therefore shallow and quick to fill) craters should overflow, which could be tested by analysis of uncommon <3.5 Ga exit-breach craters (*42*).

There is no evidence for a trend in peak runoff production with latitude. This can be understood if the paleochannel record at each latitude is a "wet-pass filter," only recording the optimal orbital conditions for runoff at that latitude, such that the latitude bands record different wet events (*37*).

DISCUSSION

Our exclusion of the hypothesis of waning peak runoff production allows an improved geologic history of peak runoff production on Mars (Fig. 5). Our results imply the following:

1) A climate-warming mechanism that allowed intense runoff production was active on Mars, at least intermittently, after 3.6 Ga and likely after 1 Ga [using the chronology of (*43*)].

2) Although we find no evidence for a reduction in peak runoff production during Mars' wet-to-dry transition, late-stage rivers are found at lower elevation and apparently exhibit stronger latitude control (*10*) than for the rivers that formed near the Noachian/Hesperian boundary. Both trends are more consistent with $\ll$1 bar atmospheric pressure than with >1 bar atmospheric pressure (*44*). This is consistent with models in which atmospheric pressure had dropped below ~300 mbar by the Late Hesperian (*2*). This is significant because many published mechanisms for early Mars' river-forming climates require atmospheric pressure $\gtrsim$ 1 bar [e.g., (*45*)].

3) Because sediment flux increases with water discharge, higher water discharges imply that the time needed to build up fluvial sediment deposits was less than for lower water discharge. For example, the eroded alcove in the northern rim of Harris crater has a volume of 7×10^9 m^3 (from our CTX DTMs). The trunk channel has a width of 50 m, a slope of 0.06, and an upstream drainage area of 4×10^7 m^2. For $\tau/\tau_{cr} \sim 2$ (*30*), the time scale for fan build-up is 2×10^3 year (this minimum time scale corresponds to a grain size of 5 cm). This is <0.01% of the total time span of alluvial fan buildup (*8*), implying strong intermittency of peak runoff production. This is consistent with the inference from Mars mineralogy that wet climates on Early Mars were intercalated with long hyperarid intervals [e.g., (*12*)].

The combination of data hints at strong positive feedbacks in the Early Mars climate system. With strong positive feedbacks, intense seasonal melting (or rainfall) occurs when a climate threshold is crossed, but below the threshold, little or no melting or rainfall occurs. Possible amplifiers include self-accelerated volatilization of polar solid-CO_2 deposits (*46*), CH_4 release from clathrate hydrate breakdown, or the exponential increase in atmospheric H_2O vapor concentration with increasing temperature of surface H_2O ice-cold traps.

There are three possible solutions to the conflict between slow late-stage atmosphere removal (*2*) and the high river discharges presented here. (i) Currently accepted dates for the late-stage rivers are wrong, and the rivers date from the early era of rapid atmospheric escape to space. (ii) Late-stage atmospheric removal processes were faster than currently thought. (iii) The late-stage river-forming climates resulted from one or more mechanisms that can produce strong warming at low atmospheric pressure, such as the water ice cloud greenhouse hypothesis (*47*). Solution (ii) seems unlikely in view of results from the MAVEN (Mars Atmosphere and Volatile EvolutioN) mission and mineralogical constraints (*2*, *12*). Solution (i) cannot be excluded without radiometric dates for Martian terrains but would imply a major modification of our understanding of inner solar system chronology. The remaining possibility, solution (iii), motivates further exploration of the effect of Mars' water-ice clouds on the past greenhouse effect.

CONCLUSIONS

We use the scale of Mars rivers to weigh hypotheses about past climate. Rivers on Mars were wider than rivers on Earth for the same catchment area. This strongly suggests intense runoff production. Unexpectedly, Mars river dimensions provide evidence for intense runoff production persisting late in the wet-to-dry transition, even as deep fluvial erosion became more spatially restricted, with more arid and/or shorter wet periods. The implication that up to 1 km of erosion late in Mars' wet-to-dry transition was associated with high peak runoff production disfavors explanations for late-stage river-forming climates on Mars that require atmospheric pressure of >1 bar [e.g., (*45*)]. That is because of the difficulty of physically justifying the removal of a thick atmosphere after 3.4 Ga (*2*). If atmospheric pressure fell between the Noachian/Hesperian boundary and Late Hesperian/Early Amazonian, then the peak runoff yielded by strongly atmospheric pressure–dependent warming mechanisms should wane as well.

Explaining the high runoff production rates implied by our data makes the difficult problem of making liquid water on ~3 Ga Mars even more difficult (Fig. 4). Therefore, our results globalize and intensify the challenge set to climate modelers by Mars Science Laboratory rover results of explaining late-stage river-forming climates on Mars (*14*, *48*).

SUPPLEMENTARY MATERIALS

Supplementary material for this article is available at http://advances.sciencemag.org/cgi/content/full/5/3/eaav7710/DC1

Fig. S1. Examples of traces showing preservation quality.
Fig. S2. Details of method.
Fig. S3. Paleo-river slope data.
Fig. S4. Sensitivity tests.

Fig. S5. Discharge area scaling: Relationship between catchment-averaged runoff production, *R*, and drainage area, *A*.
Fig. S6. Regional variations in estimated runoff production.
Fig. S7. Geologic history of Mars' river runoff.
Fig. S8. Width-discharge relationships from terrestrial fieldwork and laboratory experiments.
Table S1. Table of DTMs.
Table S2. Geologic settings of study sites.
References (*49*–*52*)

REFERENCES AND NOTES

1. D. C. Catling, J. F. Kasting, *Atmospheric Evolution on Inhabited and Lifeless Worlds* (Cambridge Univ. Press, 2017).
2. B. M. Jakosky, D. Brain, M. Chaffin, S. Curry, J. Deighan, J. Grebowsky, J. Halekas, F. Leblanc, R. Lillis, J. G. Luhmann, L. Andersson, N. Andre, D. Andrews, D. Baird, D. Baker, J. Bell, M. Benna, D. Bhattacharyya, S. Bougher, C. Bowers, P. Chamberlin, J.-Y. Chaufray, J. Clarke, G. Collinson, M. Combi, J. Connerney, K. Connour, J. Correira, K. Crabb, F. Crary, T. Cravens, M. Crismani, G. Delory, R. Dewey, G. DiBraccio, C. Dong, Y. Dong, P. Dunn, H. Egan, M. Elrod, S. England, F. Eparvier, R. Ergun, A. Eriksson, T. Esman, J. Espley, S. Evans, K. Fallows, X. Fang, M. Fillingim, C. Flynn, A. Fogle, C. Fowler, J. Fox, M. Fujimoto, P. Garnier, Z. Girazian, H. Groeller, J. Gruesbeck, O. Hamil, K. G. Hanley, T. Hara, Y. Harada, J. Hermann, M. Holmberg, G. Holsclaw, S. Houston, S. Inui, S. Jain, R. Jolitz, A. Kotova, T. Kuroda, D. Larson, Y. Lee, C. Lee, F. Lefevre, C. Lentz, D. Lo, R. Lugo, Y. J. Ma, P. Mahaffy, M. L. Marquette, Y. Matsumoto, M. Mayyasi, C. Mazelle, W. McClintock, J. McFadden, A. Medvedev, M. Mendillo, K. Meziane, Z. Milby, D. Mitchell, R. Modolo, F. Montmessin, A. Nagy, H. Nakagawa, C. Narvaez, K. Olsen, D. Pawlowski, W. Peterson, A. Rahmati, K. Roeten, N. Romanelli, S. Ruhunusiri, C. Russell, S. Sakai, N. Schneider, K. Seki, R. Sharrar, S. Shaver, D. E. Siskind, M. Slipski, Y. Soobiah, M. Steckiewicz, M. H. Stevens, I. Stewart, A. Stiepen, S. Stone, V. Tenishev, N. Terada, K. Terada, E. Thiemann, R. Tolson, G. Toth, J. Trovato, M. Vogt, T. Weber, P. Withers, S. Xu, R. Yelle, E. Yiğit, R. Zurek, Loss of the Martian atmosphere to space: Present-day loss rates determined from MAVEN observations and integrated loss through time. *Icarus* **315**, 146–157 (2018).
3. J. A. Grant, S. A. Wilson, Late alluvial fan formation in southern Margaritifer Terra, Mars. *Geophys. Res. Lett.* **38**, L08201 (2011).
4. N. Mangold, S. Adeli, S. Conway, V. Ansan, B. Langlais, A chronology of early Mars climatic evolution from impact crater degradation. *J. Geophys. Res.* **117**, E04003 (2012).
5. R. M. E. Williams, J. P. Grotzinger, W. E. Dietrich, S. Gupta, D. Y. Sumner, R. C. Wiens, N. Mangold, M. C. Malin, K. S. Edgett, S. Maurice, O. Forni, O. Gasnault, A. Ollila, H. E. Newsom, G. Dromart, M. C. Palucis, R. A. Yingst, R. B. Anderson, K. E. Herkenhoff, S. Le Mouélic, W. Goetz, M. B. Madsen, A. Koefoed, J. K. Jensen, J. C. Bridges, S. P. Schwenzer, K. W. Lewis, K. M. Stack, D. Rubin, L. C. Kah, J. F. Bell III, J. D. Farmer, R. Sullivan, T. Van Beek, D. L. Blaney, O. Pariser, R. G. Deen; MSL Science Team, Martian fluvial conglomerates at Gale crater. *Science* **340**, 1068–1072 (2013).
6. R. P. Irwin, Testing links between impacts and fluvial erosion on post-Noachian Mars, in *44th Lunar and Planetary Science Conference*, The Woodlands, Texas, 18 to 22 March 2013, LPI Contribution No. 1719, pp. 2958.
7. J. M. Moore, A. D. Howard, Large alluvial fans on Mars. *J. Geophys. Res.* **110**, E04005 (2005).
8. E. S. Kite, J. Sneed, D. P. Mayer, S. A. Wilson, Persistent or repeated surface habitability on Mars during the late Hesperian–Amazonian. *Geophys. Res. Lett.* **44**, 3991–3999 (2017).
9. T. A. Goudge, C. I. Fassett, J. W. Head, J. F. Mustard, K. L. Aureli, Insights into surface runoff on early Mars from paleolake basin morphology and stratigraphy. *Geology* **44**, 419–422 (2016).
10. E. R. Kraal, E. Asphaug, J. M. Moore, A. Howard, A. Bredt, Catalogue of large alluvial fans in Martian impact craters. *Icarus* **194**, 101–110 (2008).
11. B. M. Hynek, M. Beach, M. R. T. Hoke, Updated global map of Martian valley networks and implications for climate and hydrologic processes. *J. Geophys. Res.* **115**, E09008 (2010).
12. B. L. Ehlmann, C. S. Edwards, Mineralogy of the Martian surface. *Annu. Rev. Earth Planet. Sci.* **42**, 291–315 (2014).
13. M. H. Hecht, Metastability of liquid water on Mars. *Icarus* **156**, 373–386 (2002).
14. W. E. Dietrich, M. C. Palucis, R. M. E. Williams, K. W. Lewis, F. Rivera-Hernandez, D. Y. Sumner, Fluvial gravels on Mars: Analysis and implications, in *Gravel Bed Rivers: Processes and Disasters*, D. Tsutsumi, J. B. Laronne, (Wiley, 2017), pp. 755–783.
15. R. P. Irwin III, R. A. Craddock, A. D. Howard, Interior channels in Martian valley networks: Discharge and runoff production. *Geology* **33**, 489–492 (2005).
16. S. A. Wilson, J. A. Grant, A. D. Howard, Inventory of equatorial alluvial fans and deltas on Mars, in *44th Lunar and Planetary Science Conference*, The Woodlands, Texas, 18 to 22 March 2013, LPI Contribution No. 1719, pp. 2710.
17. D. P. Mayer, E. S. Kite, An integrated workflow for producing digital terrain models of Mars from CTX and HiRISE stereo data using the NASA Ames Stereo Pipeline, in *47th Lunar and Planetary Science Conference*, 21 to 25 March 2016, The Woodlands, Texas, LPI Contribution No. 1903, pp. 1241.
18. R. M. E. Williams, R. P. Irwin III, J. R. Zimbelman, Evaluation of paleohydrologic models for terrestrial inverted channels: Implications for application to martian sinuous ridges. *Geomorphology* **107**, 300–315 (2009).
19. D. M. Burr, R. M. E. Williams, K. D. Wendell, M. Chojnacki, J. P. Emery, Inverted fluvial features in the Aeolis/Zephyria plana region, Mars: Formation mechanism and initial paleodischarge estimates. *J. Geophys. Res.* **115**, E07011 (2010).
20. D. Mohrig, P. L. Heller, C. Paola, W. J. Lyons, Interpreting avulsion process from ancient alluvial sequences: Guadalope-Matarranya system (northern Spain) and Wasatch formation (western Colorado). *Geol. Soc. Am. Bull.* **112**, 1787–1803 (2000).
21. M. R. Gibling, N. S. Davies, Palaeozoic landscapes shaped by plant evolution. *Nat. Geosci.* **5**, 99–105 (2012).
22. Y. Matsubara, A. D. Howard, D. M. Burr, R. M. E. Williams, W. E. Dietrich, J. M. Moore, River meandering on Earth and Mars: A comparative study of Aeolis Dorsa meanders, Mars and possible terrestrial analogs of the Usuktuk River, AK, and the Quinn River, NV. *Geomorphology* **240**, 102–120 (2015).
23. M. C. Malin, K. S. Edgett, Evidence for recent groundwater seepage and surface runoff on Mars. *Science* **288**, 2330–2335 (2000).
24. E. S. Kite, A. D. Howard, A. Lucas, K. W. Lewis, Resolving the era of river-forming climates on Mars using stratigraphic logs of river-deposit dimensions. *Earth Planet. Sci. Lett.* **420**, 55–65 (2015).
25. K. Bieger, H. Rathjens, P. M. Allen, J. G. Arnold, Development and evaluation of bankfull hydraulic geometry relationships for the physiographic regions of the United States. *J. Am. Water Resour. Assoc.* **51**, 842–858 (2015).
26. G. P. Williams, River meanders and channel size. *J. Hydrol.* **88**, 147–164 (1986).
27. L. B. Leopold, T. Maddock, The hydraulic geometry of stream channels and some physiographic implications (Geological Survey Professional Paper 252, USGS Printing Office, 1953).
28. E. A. Hajek, M. A. Wolinsky, Simplified process modeling of river avulsion and alluvial architecture: Connecting models and field data. *Sediment. Geol.* **257–260**, 1–30 (2012).
29. G. Parker, P. R. Wilcock, C. Paola, W. E. Dietrich, J. Pitlick, Physical basis for quasi-universal relations describing bankfull hydraulic geometry of single-thread gravel bed rivers. *J. Geophys. Res. Earth Surf.* **112**, F04005 (2007).
30. A. M. Pfeiffer, N. J. Finnegan, J. K. Willenbring, Sediment supply controls equilibrium channel geometry in gravel rivers. *Proc. Natl. Acad. Sci. U.S.A.* **114**, 3346–3351 (2017).
31. J. D. Stock, K. M. Schmidt, D. M. Miller, Controls on alluvial fan long-profiles. *Geol. Soc. Am. Bull.* **120**, 619–640 (2008).
32. M. R. Gibling, Width and thickness of fluvial channel bodies and valley fills in the geological record: A literature compilation and classification. *J. Sediment. Res.* **76**, 731–770 (2006).
33. K. L. Hodel, The Sagavanirktok River, North Slope Alaska; characterization of an Arctic stream (United States Geological Survey Open-File Report 86-267, U.S. Geological Survey), pp. 28.
34. A. M. Morgan, A. D. Howard, D. E. J. Hobley, J. M. Moore, W. E. Dietrich, R. M. E. Williams, D. M. Burr, J. A. Grant, S. A. Wilson, Y. Matsubara, Sedimentology and climatic environment of alluvial fans in the martian Saheki crater and a comparison with terrestrial fans in the Atacama Desert. *Icarus* **229**, 131–156 (2014).
35. R. A. Craddock, A. D. Howard, The case for rainfall on a warm, wet early Mars. *J. Geophys. Res. Planets.* **107**, 21-1–21-36 (2002).
36. J. M. Davis, P. M. Grindrod, P. Fawdon, R. M. E. Williams, S. Gupta, M. Balme, Episodic and declining fluvial processes in Southwest Melas Chasma, Valles Marineris, Mars. *J. Geophys. Res. Planets* **123**, 2527–2549 (2018).
37. E. S. Kite, I. Halevy, M. A. Kahre, M. J. Wolff, M. Manga, Seasonal melting and the formation of sedimentary rocks on Mars, with predictions for the Gale Crater mound. *Icarus* **223**, 181–210 (2013).
38. A. M. Palumbo, J. W. Head, Early Mars climate history: Characterizing a "warm and wet" Martian climate with a 3-D global climate model and testing geological predictions. *Geophys. Res. Lett.* **45**, 10249–10258 (2018).
39. G. D. Clow, Generation of liquid water on Mars through the melting of a dusty snowpack. *Icarus* **72**, 95–127 (1987).
40. A. D. Howard, J. M. Moore, R. P. Irwin III, An intense terminal epoch of widespread fluvial activity on early Mars: 1. Valley network incision and associated deposits. *J. Geophys. Res.* **110**, E12S14 (2005).
41. J. L. Dickson, C. I. Fassett, J. W. Head, Amazonian-aged fluvial valley systems in a climatic microenvironment on Mars: Melting of ice deposits on the interior of Lyot Crater. *Geophys. Res. Lett.* **36**, L08201 (2009).
42. S. A. Wilson, A. D. Howard, J. M. Moore, J. A. Grant, A cold-wet middle-latitude environment on Mars during the Hesperian-Amazonian transition: Evidence from northern Arabia valleys and paleolakes. *J. Geophys. Res. Planets* **121**, 1667–1694 (2016).
43. G. G. Michael, Planetary surface dating from crater size–frequency distribution measurements: Multiple resurfacing episodes and differential isochron fitting. *Icarus* **226**, 885–890 (2013).

44. R. D. Wordsworth, The climate of early Mars. *Annu. Rev. Earth Planet. Sci.* **44**, 381–408 (2016).
45. N. E. Batalha, R. K. Kopparapu, J. Haqq-Misra, J. F. Kasting, Climate cycling on early Mars caused by the carbonate-silicate cycle. *Earth Planet. Sci. Lett.* **455**, 7–13 (2016).
46. C. Sagan, O. B. Toon, P. J. Gierasch, Climatic change on Mars. *Science* **181**, 1045–1049 (1973).
47. R. A. Urata, O. B. Toon, Simulations of the martian hydrologic cycle with a general circulation model: Implications for the ancient martian climate. *Icarus* **226**, 229–250 (2013).
48. J. P. Grotzinger, S. Gupta, M. C. Malin, D. M. Rubin, J. Schieber, K. Siebach, D. Y. Sumner, K. M. Stack, A. R. Vasavada, R. E. Arvidson, F. Calef III, L. Edgar, W. F. Fischer, J. A. Grant, J. Griffes, L. C. Kah, M. P. Lamb, K. W. Lewis, N. Mangold, M. E. Minitti, M. Palucis, M. Rice, R. M. E. Williams, R. A. Yingst, D. Blake, D. Blaney, P. Conrad, J. Crisp, W. E. Dietrich, G. Dromart, K. S. Edgett, R. C. Ewing, R. Gellert, J. A. Hurowitz, G. Kocurek, P. Mahaffy, M. J. McBride, S. M. McLennan, M. Mischna, D. Ming, R. Milliken, H. Newsom, D. Oehler, T. J. Parker, D. Vaniman, R. C. Wiens, S. A. Wilson, Deposition, exhumation, and paleoclimate of an ancient lake deposit, Gale crater, Mars. *Science* **350**, aac7575 (2015).
49. B. R. Nuse, thesis, Colorado School of Mines, Golden, CO (2015).
50. J. M. Davis, M. Balme, P. M. Grindrod, R. M. E. Williams, S. Gupta, Extensive Noachian fluvial systems in Arabia Terra: Implications for early Martian climate. *Geology* **44**, 847–850 (2016).
51. M. G. Canova, J. W. Fulton, D. M. Bjerklie, USGS HYDRoacoustic dataset in support of the Surface Water Oceanographic Topography satellite mission (HYDRoSWOT): U.S. Geological Survey data release (2016); http://dx.doi.org/10.5066/F7D798H6.
52. J. A. Grim, J. O. Pinto, Estimating continuous-coverage instantaneous precipitation rates using remotely sensed and ground-based measurements. *J. Appl. Meteorol. Climatol.* **50**, 2073–2091 (2011).

Acknowledgments: We thank C. J. Duncan, M. A. Chan, J. Sneed, and S. J. Holo for aid with terrestrial analog fieldwork carried out in support of this project. We thank B. Cardenas, C. Fassett, R. Jacobsen, M. Palucis, R. M. E. Williams, and especially, J. E. Fuller of JE Fuller/Hydrology & Geomorphology Inc., who each shared unpublished work. We thank K. Edgett and Malin Space Science Systems for CTX stereo targeting of alluvial fan source regions that enhanced this study. We thank two anonymous reviewers and the Editor, B. Schoene. We thank the HiRISE team for maintaining the HiWish program, which provided multiple images that enhanced this study. We acknowledge useful discussions with D. Burr, B. Cardenas, R. diBiase, C. Fassett, C. Gleason, T. Goudge, J. Grant, A. Hayden, J. Head, A. Howard, R. P. Irwin, R. Jacobsen, D. Jerolmack, L. Karlstrom, J. Kirchner, N. Mangold, T. Minear, D. Mohrig, J. Moore, A. Morgan, P. Nelson, G. Parker, T. Pavelsky, A. Pfeiffer, and H. J. Seybold. We thank C.B. Phillips for aid with DTM production. **Funding:** This study made use of University of Chicago Research Computing Center resources. Grants: NNX15AM49G and NNX16AG55G (both from NASA), ST/K502388/1 (STFC), and ST/R002355/1 (UK SA). **Author contributions:** E.S.K. conceived, designed, and carried out research, and wrote the paper. D.P.M. constructed DTMs and built and managed the Geographic Information System for this project. J.M.D. and A.S.L. constructed DTMs. S.A.W. contributed a global database of Mars deltas and alluvial fans. G.S.d.Q. carried out the minimum formation time scale calculations. **Competing interests:** The authors declare that they have no competing interests. **Data and materials availability:** All shapefiles and all MATLAB scripts may be obtained from the lead author for unrestricted further use. All DTMs are also available for unrestricted further use (see table S1 for details).

Submitted 26 October 2018
Accepted 8 February 2019
Published 27 March 2019
10.1126/sciadv.aav7710

Citation: E. S. Kite, D. P. Mayer, S. A. Wilson, J. M. Davis, A. S. Lucas, G. Stucky de Quay, Persistence of intense, climate-driven runoff late in Mars history. *Sci. Adv.* **5**, eaav7710 (2019).